# Efficient algorithms for the study and design of parallel robotic mechanisms with physiotherapy applications

Christos E. Syrseloudis*
National and Kapodistrian University of Athens
Department of Informatics and Telecommunications
15784 Athens Greece
chsirsel@di.uoa.gr

**Abstract**

The aim of this work is to study the design and identification of kinematics parameters of robotic mechanisms for ankle physiotherapy applications. We begin with the study of the ankle joint complex and we adopt the 2 axes kinematics model from the literature which provides the necessary DOFs and the kind of the ankle motions. The objective is to describe the basic movements of the foot about the ankle joint. We accomplish the design requirements of a physiotherapy robot by performing appropriate experimental measurements. These requirements are the necessary workspace, velocities, accelerations and torque bounds. We examine two existing robotic architectures while we finally introduce a new 2-DOF hybrid serial-parallel robot with mechanical adjustability as an ankle physiotherapy device. The advantages of this physiotherapy device against the existing physiotherapy robots are the minimum number of its actuators, its increased safety, modularity and economy. Then we perform the parametric design of this platform which has been based on the predefined design specifications and then we evaluate the design via simulations. Finally, we develop a simple, accurate and robust identification method of the kinematics parameters of the ankle joint complex. This method combines the concept of robot calibration and arc trajectory fitting in 3D circles.

## 1 Introduction

In this dissertation we focuss on the design and identification of kinematics parameters of robotic mechanisms for ankle physiotherapy applications. Our contribution is in the following three main topics:
-*Design framework*: A unified design framework for the design of an ankle rehabilitation robot is missing from the literature. We study the ankle kinematics modeling and we complete with experimental data a set of design requirements for an ankle rehabilitation robot.
-*Design of a new ankle rehabilitation robot*: The existing ankle rehabilitation robots are either redundant or not follow exactly the ankle movements. The detailed study of the ankle kinematics led us to introduce a new hybrid parallel-serial robot with 2-DOF and mechanical adjustability. The parametric design of the new robot is carried out relying on the design specification described above. This physiotherapy device outperforms to the existing physiotherapy robots on the minimum number of actuators, safer movements, modularity and economy.
-*Identification of the ankle joint complex kinematics*: The different kinematics characteristics between patients reveal the need for identification of the ankle parameters for the appropriate tuning of a physiotherapy robot. We develop a simple and robust method for identification of the ankle joint kinematics which combines the concept of robot calibration and arc trajectory fitting in 3D circles. Despite to the existing identification methods, our method avoids the use of position tracking of multiple point-markers on the body-member and the use of expensive optical motion analysis systems. This makes it applicable in a physiotherapy clinic.

### 1.1 Previous Work

Our study begins with the structure and kinematics modeling of the ankle joint complex. The human ankle has a complex multi-joint structure which determines the motion of the foot with respect to the shank. A survey in [7] about the ankle-joint complex modeling starts with early

*Dissertation advisor: Ioannis Z. Emiris, Professor.

models, e.g. spherical joint and concludes with recent work e.g 4-bar modeling. In particular, certain advanced models incorporated the early findings of the two anatomical joint axes in the ankle, namely the upper ankle and the subtalar joint axis. In [8] was applied a 2-DOF (Degree Of Freedom) model to the lower leg, namely as a linkage of two ideal revolute joints and 3 rigid segments: the shank, the talus and the foot. The orientations axes could be determined by anatomical landmarks on the bones. In [1] were identified two subject-specific, fixed joint axes in the ankle complex by applying least-square optimization to minimize the difference between the real motion of external skin markers and the modeled motion. They noticed the relatively high variability between subjects especially of the subtalar and upper ankle joint orientation. Recently, a model that does not imply the existence of two distinct axes of the ankle joint complex and forms an innovative category of its own, have formulated a 2-dimensional model of the upper ankle joint by representing it as a closed 4-bar linked chain.

In closer detail, the ankle joint shows a mobile axes with a predetermined (1-DOF) path during passive flexion, but when loads are applied (e.g. muscle contraction), the mobile axes can deviate from this passive path, while the subtalar joint plays a stabilizing role. In our work, this deformable modeling is not required: the two-axes model represents the main movements and the kinematics of the ankle joint sufficiently well, and is quite accurate for our purposes. This has been proved in [16], in which was studied the use of the 2-axes ankle model and the identification procedure presented in [1] for calculation and comparison of the two hinge axes of the ankle joint complex for non-weight-bearing, weight-bearing and walking ankle motions. It was found that the 2-axes model fits the experimental data well with non-weight-bearing motion achieving the best fit. Since physiotherapy exercises especially in the early steps contain non-weighting-bearing movements the 2-axes model is sufficient for ankle modeling.

There have been a number of robotic devices proposed for ankle physiotherapy. Important work has been carried out at Rutgers University [10] with the development of a haptic interface for human ankle rehabilitation. This haptic interface has been based on a 6-DOF Stewart platform that applies variable forces and virtual reality exercises on the patient's foot, including remote control operation. However the Stewart platform is redundant for this application, the actuators used are noisy, the controller is oversized and the cost of the device is consequently high. In addition, in the rehabilitation program, there is no reference as to what extent the special characteristics of each patient's foot can be considered. Also the work in [3] is based on the study of ankle functional anatomy, which is represented in an orientation image space. Three parallel tripod-type ankle rehabilitation mechanisms were proposed. These are three or four actuator platforms and therefore they are redundant. Also, the rotation of the moving platform is performed about a vertical pivot strut, which is not a desirable characteristic for foot movements. In [27] was proposed an ankle rehabilitation device based on a reconfigurable parallel robot with 4-DOF and two moving platforms. However, this platform is quite complex and heavy and as a result is rather difficult in construction and transfer. A 2-DOF redundantly actuated parallel mechanism for ankle rehabilitation was proposed in [19]. The proposed device allows plantar- dorsiflexion and inversion-eversion using actuation redundancy to eliminate singularity, and to improve the workspace dexterity. However, this device is over-actuated, which means that there are redundant actuators.

The next important problem studied here is to determine the kinematics parameters of the ankle joint complex. Ankle joint complex kinematics is similar with that of a 2R serial manipulator (R denotes a revolute joint)[2] and therefore we approach the identification problem as a serial manipulator calibration problem. Identification of the axes of rotation of the limb-joints, by tracking specific point-markers on the body member, has received significant attention. In [1] was used the 2-axes model and identified the twelve parameters of an ankle joint complex model which is based on transformation matrices. This method requires the assignment of at least 3 non-collinear point-markers on each limb segment and tracking by the use of optical motion analysis systems. In [11] was proposed a least squares method by minimizing specific cost functions formed by the vector differences of the points markers positions. One drawback of the method is that for certain configurations of point markers (e.g. the markers distributed on a plane that contains the rotation axis) leads to ill-conditioned problems. Also, in [9] was presented a least squares method for average center and axis of rotation estimation. This method does not perform well if there is significant radial displacement from the center of the axis of rotation and needs at least three non-planar markers in general. These methods rely on position tracking of multiple point-markers which are assigned on the body by the use of expensive optical motion analysis systems.

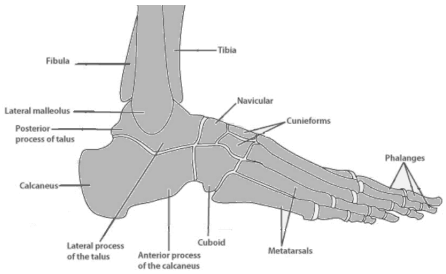


*(a)* Foot anatomy and bones.

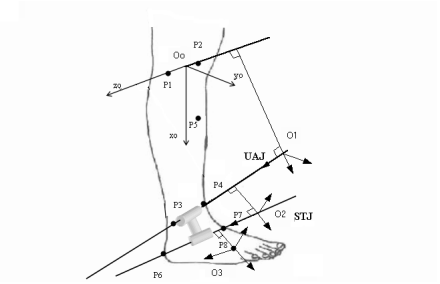


*(b)* Ankle rotation axes and the assigned D-H frames.

Figure 1: The ankle joint complex anatomy and kinematics.

# 2 Design specifications for an ankle rehabilitation robot

In order to design a robotic physiotherapy device the first step is to define the necessary design framework. For this we begin with the kinematics modeling of the ankle joint complex and we complete the design requirements with experimental data.

## 2.1 The ankle joint complex kinematics

The human ankle has a complex multi-joint structure. The central bone is the talus. Its surrounding bones are the calcaneus, the navicular and the cuboid; they are responsible for the rotation of the ankle joint in 3D (fig. 1(a)). The upper part of the talus articulates with the shank segment through the tibia and fibula bones. This is the upper ankle joint (UAJ); it supports the rotational dorsiflexion-plantarflexion motion. The movements between the fore bones are strictly coupled. Motion of the foot wrt the talus is regarded as a rotation about the (fixed) subtalar axis (STJ); this supports inversion-eversion motion.

Among previous works, the early single-joint models are insufficient while the recent models do not fully describe foot rotations (e.g. they may consider only dorsiflexion-plantarflexion). Here we adopt the ankle joint complex model as a 2R serial manipulator [8], assuming the ankle rotation axes are straight lines through specific points. The lower limb is assumed to be composed of 3 rigid links capable to rotate between each other: the shank, the talus and the foot configuring a serial manipulator. The main movements of the foot are the plantarflexion-dorsiflexion and inversion-eversion. The size of foot bones and their relative positions as well as the orientation of rotation axes determine the foot kinematics. Many factors influence the joint rotation, e.g. shape of articular surfaces, position of rotation axes. Constraint and resistance on the foot motions are due to ligaments, capsules and tendons.

The parameters of this model are specified by a number of point markers that have been assigned on the human foot as in fig. 1(b). These point markers are used to obtain a set of distance measurements. We assign frame $O_1$ at the knee, centered between $P_1, P_2$, with the $z$-axis parallel to $(P_1, P_2)$ and the $x$-axis vertical, passing through the midpoint of $(P_3, P_4)$. By using the Denavit-Hartenberg(D-H) method [12, 22] we assign relative frames $O_i$ between the moving links. $T_i^{i+1}$ is the transformation matrix from $O_i^{i+1}$ into $O_i$. The transformation matrix from the last into the first coordinate system is given from the relationship: $T_1^3 = T_1^2 T_2^3$. For a point $P = [x\ y\ z\ 1]^T$ on the last(foot) coordinate system the above transformation into the first(shank) coordinate system can be expressed as $P_o = [x_o\ y_o\ z_o\ 1]^T$:

$$P_o = T_1^3 P \tag{1}$$

from which the coordinates $x_o, y_o, z_o$ are nonlinear functions $f_i(a_i, \alpha_i, d_i, \vartheta_i, x, y, z)$ of the D-H parameters $a_i, \alpha_i, d_i, \vartheta_i$. These equations give a parametric formula in the movement of $P$ wrt the fixed coordinate system of the shank. The independent variables of the model are angles $\vartheta_2$ (dorsiflexion-plantarflexion), $\vartheta_3$ (inversion-eversion) while $\vartheta_1$ is constant. According to the right-hand coordinate system assigned to the lower limb, the signs for rotation angles are: dorsiflexion(+), plantarflexion(-), eversion(+) and inversion(−). Movements of the left leg are assumed to be the mirror-image of the right leg [8]. The parameters $\alpha_i, a_i, d_i$ depend on the foot anatomy and size.

The transformation matrices were estimated for a male subject, and distances between the bony landmarks taken from [8]. From this data, a kinematics model of the foot was based on homogenous matrix transformations in Euler angles. Using calculations on the distances, we

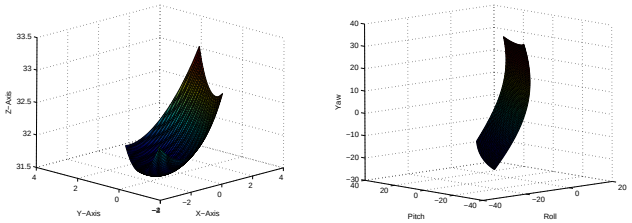


*(a)* Translation *(b)* Rotation

Figure 2: Workspace from a point on the sole under the ankle.

obtain the D-H parameters. From the above analysis, the knee axis have angle $38.23^o$ with the UAJ and the UAJ with the STJ have angle $60.21^o$.

We take $\vartheta_{dp}$, $\vartheta_{ie}$ as the new variables for the dorsiflexion-plantarflexion and inversion-eversion angles measured from the standing posture, and insert $\vartheta_2 = \vartheta_2^o + \vartheta_{dp}$, $\vartheta_3 = \vartheta_3^o + \vartheta_{ie}$ into eqts (1). Now $\vartheta_{dp}$, $\vartheta_{ie}$ are the input variables of the model. Common ranges for the movement are $-40^o \leq \vartheta_{dp} \leq 30^o$, $-20^o \leq \vartheta_{ie} \leq 20^o$ [22]. Based on the model, we specify the foot workspace when inputs range through all possible motions. Our first requirement is the shank to be fixed and vertical wrt the World Coordinate system attached to the base of the robot.

We fix point $P_f$ on the sole under the ankle where the center of the moving platform will be attached. We assume $P_f$ is on the positive axis of the knee's frame and has a distance equal to this of $P_6$. The workspace produced by the foot will be derived from the motion study of $P_f$. By eqts (1) and letting inputs $\vartheta_{dp}, \vartheta_{ie}$ run through their entire regions, $P_f$ traces the surface of fig. 2(a). Feet of every size and anatomy produce the surface in fig. 2(a). The geometric characteristics of this surface (e.g. shape, curvature), depend on $\alpha_i, a_i, d_i$. Every trajectory traced by $P_f$ is within this surface.

Table 1: Coordinate ranges of a point on the sole under the ankle.

| ΔX=56 mm | | ΔY=41.7 mm | | ΔZ=17.3 mm | |
|---|---|---|---|---|---|
| Min X | Max X | Min Y | Max Y | Min Z | Max Z |
| -33.5 | 22.4 | -19.6 | 22 | -2.8 | 14.4 |

We compute the orientation of the foot when its axes are rotated in specific angles. First, we establish a reference frame with its origin at $P_f$. The axes are parallel with those of the base frame when the foot is in the neutral position. The rotation angles roll($\alpha$), pitch($\beta$), yaw($\gamma$) of this frame wrt the base frame are the rotation angles of the moving platform. The foot model, when $\vartheta_{dp}$, $\vartheta_{ie}$ take all values in their ranges, yield the rotation workspace in fig. 2(b). By

Table 2: Orientation ranges based on the model.

| $\Delta\alpha$=30.56 deg | | $\Delta\beta$=76.58 deg | | $\Delta\gamma$=62.49 deg | |
|---|---|---|---|---|---|
| Min $\alpha$ | Max $\alpha$ | Min $\beta$ | Max $\beta$ | Min $\gamma$ | Max $\gamma$ |
| -20.71 | 9.84 | -39.95 | 36.63 | -25.34 | 37.15 |

assuming that the angle axes parameters in eqts (1) are found in well specified intervals, we will specify the extended workspace produced by the model (eq. (1)). In [14], the orientation of the lower limp rotation axes, and the ranges in the relevant angles between them are measured. The results depend on the position of the foot even for a given patient. Different patients will give different results. We conclude that the model parameters are quite uncertain and so the model must be extended to include uncertainties. By computing the minimum and maximum values we take the values in table 3.

## 2.2 Experimental data

A Mephisto 3D Scanner was used to take images of the right foot sole of 11 adult healthy human subjects of different age, height, weight and gender. We used 5 positions: Neutral, Right-Up, Right-Down, Left-Up and Left-Down. The reference is a central point on the sole under the ankle because this point will be controlled by the platform. The coordinate differences among

Table 3: Extended coordinate ranges of a point on the sole under the ankle.

| ΔX=114.2 mm | | ΔY=98.9 mm | | ΔZ=37.3 mm | |
|---|---|---|---|---|---|
| Min X | Max X | Min Y | Max Y | Min Z | Max Z |
| -67.6 | 46.9 | -4.55 | 53.4 | -7.6 | 29.7 |

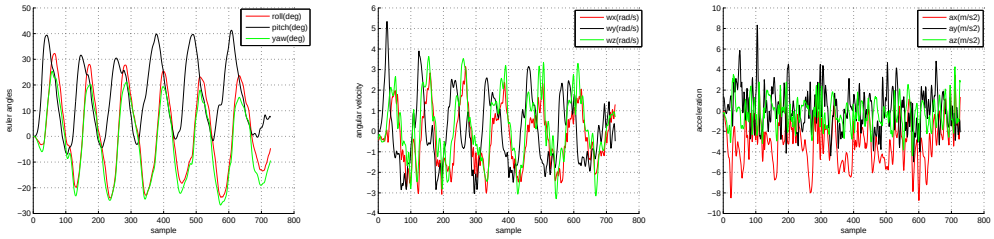


*(a)* Euler angles *(b)* Angular velocities *(c)* Linear accelerations

Figure 3: Recorded data in full rotations of the foot.

the point's positions are found inside the following enclosing volume: ΔX=12cm , ΔY=12 cm, ΔZ=12 cm.

To measure orientation angles, rotation velocities, and accelerations, we performed experiments with an MTi motion sensor of XSens Motion Technologies. It provides and records pitch, roll and yaw angles, rate of turn and linear accelerations in axes $X, Y, Z$. We used the right foot of 5 adult healthy humans of both genders and different heights, with the shank kept vertical and fixed. The only moving part was the foot. The sensor was attached on the sole of the foot under the ankle. Data were recorded during dorsiflexion-plantarflexion and inversion-eversion throughout the entire range of movement. Fig. 3(a) shows roll, pitch and yaw wrt time of a foot, in extreme rotational movement. Fig. 3(b) shows angular velocities wrt time in extreme rotational movement while fig. 3(c) shows linear accelerations wrt time in extreme rotational movement. The maximum recorded angular velocity was 9.3rad/sec and therefore the upper bound of 10 rad/sec is adopted.

The torque bounds are coming from the literature in which they studied the tension torque that the soleus and tibialis anterior muscles can exert. These are two of the main dorsiflexor-plantaflexor muscles and the maximum measured torque was about 121Nm. Also, in another work the maximum measured torques of the whole plantarflexor and dorsiflexor muscle groups were about 143Nm [22, 24]. Therefore a desired upper bound of 200Nm includes a wide range of foot torque capabilities. Thus, our platform will operate up to 200Nm, to handle torque-producing tasks at different velocities during concentric or eccentric muscle actions.

# 3 Design of a 2-DOFs hybrid parallel-serial ankle physiotherapy robot

Initially, we studied two existing robotic architectures as possible ankle physiotherapy devices [23]. The first one was the Agile Eye. Although the Agile Eye has only 3 rotational DOFs and large workspace, its sensitivity to transfer and its rotations about only one point led us to reject this robot. The second one was a parallel Tripod(3-RPS) with an extra rotation axis on the moving platform as a possible ankle rehabilitation device was studied in . The Tripod has two rotational (pitch, roll) and one translational (z) degrees of freedom. As the yaw angle changes significantly during the foot movements on the platform, an extra rotation axis was added on the moving platform to provide the necessary extra yaw angle. Although this device can not follow the foot movements satisfactorily or include mechanical adjustability and our effort is to design a robot with fewer DOFs.

To overcome the previous disadvantages we proposed a hybrid serial-parallel robotic architecture with 2-DOF and mechanical adjustability [24]. The robot consists of a base platform and a moving platform like most parallel robots. The latter is where the patient's foot shall be placed. A vertical strut connects the base of the robot with a passive serial chain. The serial chain has structure similar to that of the foot and provides the necessary constraints on the movements. It has one revolute and one cylindrical joint which support the rotations about the two main rotation axes of the ankle, see Figure 4. $R_1$ is a revolute-joint which is collinear with

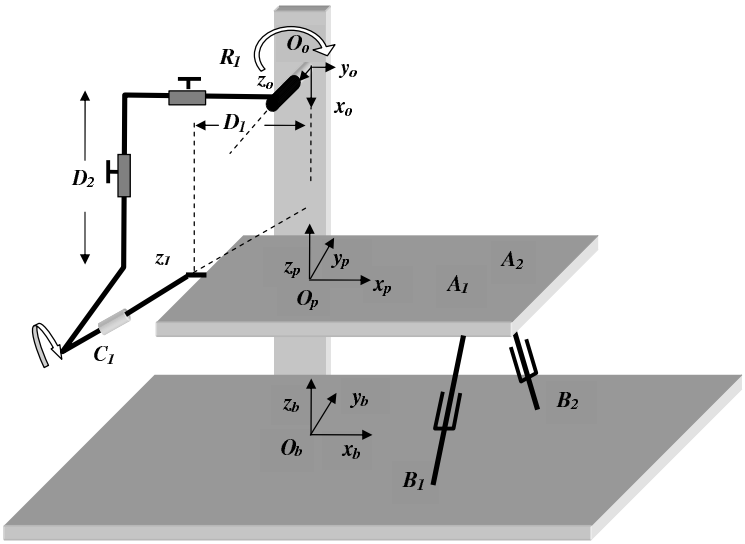


Figure 4: The hybrid serial-parallel 2DOF ankle physiotherapy robot.

the Upper Ankle Joint (UAJ) and $C_1$ is a cylindrical-joint which is collinear with the Subtalar Joint (STJ) of the foot. The serial chain is connected with the moving platform and has two adjustable screws so that the corresponding lengths $D_1$, $D_2$ can be adjusted according to the axes position of each individual patient's foot. The parallel chain consists of two prismatic actuators which are connected with the moving platform through S-Joints (points $A_1$, $A_2$) and with the base platform through U-Joints (points $B_1$, $B_2$).

## 3.1 Kinematics modeling of the platform

We start by modeling the kinematics of our device. The mobility of the platform is modeled by applying the Grubler formula for spatial structures. The total number of its degrees of freedom N is given as follows: $N = 6(n-j-1) + \sum_i^n f_i = 6(8-9-1) + 14 = 2$, where n represents the total number of rigid bodies of the mechanism, including the base, j is the total number of joints, and $f_i$ the number of degrees of freedom of joint i. Initially we assign the base coordinate frame $O_b x_b y_b z_b$ on the fixed base and the moving frame $O_p x_p y_p z_p$ on the moving platform as shown in figure 4. The two frames are parallel when the moving platform is in zero position. As we have a serial kinematics chain it is useful to implement the Denavit-Hartenberg method [12] for the assignment of the relative reference frames on the passive serial chain and therefore to obtain the overall kinematics formula of the platform. The $O_o x_o y_o z_o$ frame is the base frame of the serial chain and is placed arbitrarily on the strut with the axis $z_o$ collinear with the UAJ axis, and $x_o$ collinear with $z_b$, as shown in Figure 4. The origin $O_2$ of the $O_2 x_2 y_2 z_2$ frame is the $O_p$ of the platform frame and the axis $z_2$ is parallel with $z_1$ ($C_1$). The total transformation matrix T is given by the multiplication: $T = T_b T_0^1 T_1^2 T_r$, where $T_b$ is a constant homogeneous rotation matrix defining the relative rotation of the $O_o x_o y_o z_o$ frame into the base $Ob_x b_y b_z b$ frame. The points on the platform coordinate frame need to be multiplied with an extra rotation matrix $T_r$ in order to be transformed into the last D-H frame of the serial chain. The inverse kinematics problem is described from the following two equations:

$$L_i^2 = \|B_i A_i\|^2 = \|T \cdot A_i - B_i\|^2, \tag{2}$$

where i=1,2 and $L_i$, are the length of the actuated links. It is well known that the Jacobian matrix is a key part for the study and design of robots. By following the normalized Plucker vector-based procedure for the inverse Jacobian calculation of a general parallel robot as it is described in detail in [18] we get:

$$J^{-1} = \begin{bmatrix} n_1 & n_1 \times A_1 O_p \\ n_2 & n_2 \times A_2 O_p \end{bmatrix}, \tag{3}$$

where $n_1$, $n_2$ are the unit vectors of $B_1 A_1$, $B_2 A_2$.

## 3.2 Velocity and Force Transmission

When the linear actuators are activated their velocities and applying forces are transferred onto the moving platform. The relations between the forces-velocities of the actuators and

the moving platform are expressed by the Jacobian matrix and are pose-dependent. Here we follow the kinetostatic capability analysis of parallel manipulators described in [15] where the calculation of the magnitude bounds of the force and velocities of the end-effector is reduced to an eigenvalue problem. Matrix M is essential here and is defined as follows:

$$M = J^{-T}J^{-1} = \begin{bmatrix} A & B \\ B^T & C \end{bmatrix} \tag{4}$$

Given the desired velocities as well as the force and moments that should be handled by the platform, the extreme values of the velocities and forces of the linear actuators are computed in the design phase. The linear forces and torques have different units it is reasonable for the bounds computation of force-torques at the end-effector to be decoupled into two constraint maximization subproblems, one for the forces f and one for the torques m. By use of matrix M the two maximization subproblems can be rearranged into eigenvalue subproblems. Following a similar procedure as in the force transmission analysis, velocity transmission analysis is decoupled in two subproblems, one for the linear $\nu$ and one for the angular $\omega$ velocities magnitudes.

$$\frac{\|f\|}{a_{fmax}} \leq \|\tau\| \leq \frac{\|f\|}{a_{fmin}}, \quad \frac{\|m\|}{a_{mmax}} \leq \|\tau\| \leq \frac{\|m\|}{a_{mmin}} \tag{5}$$

$$a_{\nu min}\|\nu\| \leq \|\dot{L}\| \leq a_{\nu max}\|\nu\|, \quad a_{\omega min}\|\nu\| \leq \|\dot{L}\| \leq a_{\omega max}\|\nu\| \tag{6}$$

where A, C are the $3 \times 3$ submatrices of M and $\nu$, $\omega$ the $3 \times 1$ vectors of linear and angular velocities of the end-effector, f, m the $3 \times 1$ vectors of linear forces and torques on the end-effector. The bounds of the velocities magnitudes are therefore given from the inequalities where $a\nu_{max}$ and $a\nu_{min}$ denote the square roots of the maximum and minimum eigenvalues of A, and $a\omega_{max}$ and $a\omega_{min}$ are those of the maximum and minimum eigenvalues of C. By discretizing the whole workspace of the robot and computing the global extreme eigenvalues of M, the global magnitude bounds of velocities and forces are computed.

### 3.3 Parametric Design of the Robot

This section presents the parametric design of our mechanism, since we have chosen the robotic architecture. Design concerns the calculation of the geometric parameters of the robot satisfying our requirements [18]. Based on the above foot analysis, the following values were selected for initial dimensioning of the device: Moving platform: 0.40x0.20m so that it can accept all or at least the majority of human foot sizes. Base platform: 0.60x0.40m. The first axis zo is placed 50cm above the fixed base. The bounds of rotation axes of the serial chain were defined according to the range of the feet rotations. The STJ axis, and so the z1 has the mean foot orientation as it is given and forms an angle of $23^o$ with the $x_pz_p$ plane and an angle of $41^o$ with the $x_py_p$ plane. This work has been extended and in order to complete the design of the robot, additional measurements on the foot of several human subjects have been conducted. Coordinates of specific points of the foot, have been measured, utilizing a Microscribe coordinate measuring device. For the experimental measurements the right feet of 19 adult males and females have been used in the erect standing pose. The UAJ is defined by points $P_3$ (lateral malleolus) and $P_4$ (medial malleolus), while the STJ is defined by points $P_6$ (calcaneus point) and $P_7$ (navicular point). For calculating the bounds on distance $D_1$ the points $P_3$, $P_4$ and $P_6$ were projected on the horizontal plane. The vertical distance of the projected point $P_6$ from the projected line $P_3P_4$ defines distance $D_1$. The computed values of $D_1$ were found to be in the range: $3.5cm \leq D_1 \leq 5.6cm$, with mean value 4.83cm and standard deviation 0.68cm. For calculating the range of distance $D_2$, the mean value of the height of points $P_3$ and $P_4$ from the horizontal plane was computed. The resulting values are in the following range: $5.4cm \leq D_2 \leq 9.3cm$, with mean value 7.29m and standard deviation 1.02cm. Points $A_1$, $A_2$ on the moving platform have been assigned coordinates (0.15,-0.06,0) and (0.15,0.06,0) of the moving frame respectively. If the points are far from the rotation axis then the actuators apply smaller forces but larger velocities. Reversely, if the points are near the rotation axis then the actuators apply forces with larger values and smaller velocities. Therefore, the points are selected to be in the middle of the platform in order to balance the amounts of the velocities and forces exerted by the actuators. The coordinates of the base platform points $B_1$, $B_2$ have been assigned to (0.10,-0.15,0) and (0.10,0.15,0) respectively, on the base reference frame nearer to the origin so to avoid singularities. The coordinate units are in m. When the platform moves through the entire range of rotations and parameters $D_1$, $D_2$ take all values in the above intervals, then the length of the legs are found in the range: [0.31m, 0.56m]. Having computed the kinematics

parameters of the robot as well as the desired end-effector velocities and wrench forces, the actuator velocities and forces can be computed. The platform must handle torque values up to 200Nm. In order for the platform to achieve these torque bounds, the actuator forces must be greater than 675N according to equation (5). Similarly, for velocities calculation used the upper bounds of 10rad/sec in angular velocities of the platform. According to equation (6), the linear actuators should achieve velocities at least 2.1m/sec in order characteristics providing the robot motion can be selected. Simulations with the maximum design values movements shows that the platform fulfils the design requirements, proving the succeed of design [24].

# 4 Identification of the ankle joint complex kinematics

For the identification of the ankle joint complex kinematics parameters it is useful to implement robot calibration techniques. Since the internal joint ankle values is difficult to be measured, conventional calibration techniques are not applicable. Therefore, we approach the problem by trying algebraic elimination and trajectory fitting in 3D circles [21].

## 4.1 Algebraic methods

We first approached identification via algebraic variable elimination. Algebraic elimination of the two rotation angles of the ankle might be a reliable approach, just as it has been for parallel robots [4, 5]. However, the case of serial robots presents certain difficulties compared to parallel robots. In the latter case, the kinematics equations are produced by one multiplication with one homogeneous transformation matrix. In serial robots, the kinematics equations are obtained by successive multiplication with as many homogeneous matrices as the number of links. Hence, the final kinematics equations are quite complex [21].

One approach is to linearize the polynomial system by resultants. It is typically expressed as a matrix determinant, and the resultant matrix can be used to reduce system solving to a problem in linear algebra [6]. In the case of a manipulator with two revolute joints, its kinematics model is the product of two D-H matrices. To eliminate the two rotation angles by resultants, the *mresultant* function of MAPLE package *Multires* yields a $21 \times 21$ matrix which contains polynomials of degree up to 15, therefore the determinant is very hard to compute.

## 4.2 Identification by nonlinear fitting in 3D circles

This section presents identification without using internal joint values, based on fitting 3D circles. Let us consider a serial manipulator with only revolute joints, where all the joints are fixed in their zero position. Starting from the last axis we rotate it and record the Cartesian position of the end-effector. After we fix the last axis, we rotate the previous axis while all the remaining axes are unmovable in the zero position and record the end-effector's positions. We repeat until the rotation of the end-effector about the first axis is recorded. Rotation of a point about an arbitrary axis in 3D traces a circular arc. Given $N$ measured points of the arc, we estimate the parameters (center, radius, normal) in two steps: (1) the points are fitted on the plane of the arc, while the plane-normal defines the rotation axis, (2) we compute the center and radius of the arc.

Nonlinear least-squares minimize $f = \sum_{i=1}^{N} e_i^2$, where the $e_i$ denote the errors, by iteratively linearizing around the parameters the following:

$$\Delta f = J_k \Delta x, \tag{7}$$

where $\Delta f$ is the error between measured and residual function, $\Delta x$ is the correction of parameter vector $x$ in the current estimate, and $J_k$ is the identification Jacobian. Usually, weighting of least-squares gives better accuracy and is achieved by task variable and column scaling. The measured data are of the same units and therefore task variable scaling via noise covariance matrices is not necessary. On the other hand, column scaling improves the condition number $\kappa = \sigma_1/\sigma_p$, where $\sigma_1$ is the largest and $\sigma_p$ the smallest nonzero singular values of $J_k$. Column scaling does not affect the solution and is achieved by right multiplication of $J_k$ by matrix $H = diag(h_1, \ldots, h_n)$ with

$$h_i = \begin{cases} ||J_{ki}^{-1}||, & \text{if } ||J_{ki}|| \neq 0, \\ 1, & \text{if } ||J_{ki}|| = 0\ , \end{cases} \tag{8}$$

where $J_{ki}$ is the $i$-th column of $J_k$. With column scaling the singular values of $J_k$ become comparable. Studying $J_k$ before the actual identification, provides information about identifiability and the observability.

*a) Identifiability:* This determines whether all parameters can be identified independently, or some are non-identifiable because depend on others. Non-identifiable parameters exist if $J_k$ is rank deficient. In this case, several approaches have been proposed [13] for identification: (i) elimination of the non-identifiable parameters by QR decomposition (ii) zeroing small singular values, and (iii) incorporating a priori estimates, where small or zero singular values are counteracted by a constant weighting factor. An efficient technique we use here is (ii), which identifies without removing any parameter or a priori estimates. Our method begins with singular value decomposition (SVD) of scaled matrix $J_k = U\Sigma V^T$, where $U$ is $N \times N$ orthogonal, $V$ is $n \times n$ orthogonal, and $\Sigma$ is $N \times n$ diagonal, with singular values $\sigma_1 \geq \cdots \geq \sigma_p > 0 = \cdots = 0$. If $p < n$, then $J_k$ is rank deficient so each iteration step of 7 computes

$$\Delta x = \sum_{j=1}^{n} \frac{u_j^T \Delta f \, v_j}{\sigma_j}, \tag{9}$$

where, if $\sigma_j$ is zero or numerically small, we set $1/\sigma_j = 0$.

*b) Observability:* Observability concerns the selection of the best measurement sets according to an observability index. Several observability indices which indicate the measurements of high accuracy have been proposed. A very interesting one is the *noise amplification index* $O = \sigma_p^2/\sigma_1$ , which relates the amplification of the measurement noise with the estimated parameters. It is more sensitive to measurement and modeling error than previous indices. The measurement poses set with larger $O$ results to a more accurate identification.

*Step 1*: The coordinate data will be fitted to the 4 parameter plane: Ax+By+Cz+D=0. The vertical distance $d_i$ of a 3D point $i$ from a plane is given by:

$$d_i = \frac{Ax_i + By_i + Cz_i + D}{\sqrt{A^2 + B^2 + C^2}}. \tag{10}$$

We have to minimize the objective: $f_d = \sum_1^N d_i^2$. Identification is performed after certain iterations of linear least-squares 7. The identification Jacobian is the stacked matrix for all measurements of the rows $J_k^l$ of the following derivatives : $J_k^l = \left[ \begin{array}{cccc} \frac{\partial d_i}{\partial A} & \frac{\partial d_i}{\partial B} & \frac{\partial d_i}{\partial C} & \frac{\partial d_i}{\partial D} \end{array} \right]$.

*Step 2*: The arc points are projected onto the plane by computing a verticality condition. The center and radius of the arc is defined by an intersecting sphere with the resulting plane of *Step 1*. The residuals of the sphere and measured data points are: $e_i = (x_i - x_c)^2 + (y_i - y_c)^2 + (z_i - z_c)^2 - R^2$. Therefore, to find the best fitting sphere, we solve the constrained nonlinear least-squares: $f_e = \sum_1^N e_i^2$, subject to: $h(x_c, y_c, z_c) = Ax_c + By_c + Cz_c + D = 0$. Similarly with the linearized procedure of *Step 1*, the constrained nonlinear least-squares can be solved by iteratively solving:

$$\begin{bmatrix} -J_s^T J_s & J_h^T \\ J_h & 0 \end{bmatrix} \cdot \begin{bmatrix} p_k \\ \lambda_k \end{bmatrix} = \begin{bmatrix} J_s^T e_i \\ -h \end{bmatrix}, \tag{11}$$

where $J_s$ the identification Jacobian, namely the stacked matrix for all measurements of the rows $J_s^l$ of the following derivatives of the residuals:$J_s^l = \left[ \begin{array}{cccc} \frac{\partial e_i}{\partial x_c} & \frac{\partial e_i}{\partial y_c} & \frac{\partial e_i}{\partial z_c} & \frac{\partial e_i}{\partial R} \end{array} \right]$, where matrix $J_h$ is the Jacobian of the constrained equation $h$ with respect to the parameters $(x_c, y_c, z_c)$, $p_k = [x_c, y_c, z_c, R]$ is the vector of estimated parameters, and $\lambda_k$ is the scalar Lagrange multiplier for the constraint. The two steps yield the circle center $p_c = (x_c, y_c, z_c)$, radius $R$, as well as the normal vector $\overrightarrow{n}$, which is the unit vector of $\overrightarrow{p} = [A, B, C]$.

## 4.3 Identification by linear fitting in 3D circles

We follow the previous two-steps procedure of fitting the plane and circle but avoid to use non-linear least-squares.We employ direct methods which are computationally faster and accurate.

*Step 1*: The plane is estimated via SVD [20]. Let $p_p$ be a point on the best fitted plane, $p_i$ a given point, and $\vec{a}$ the normal vector to the plane. The vertical distance of $p_i$ from this plane is $d_i = \vec{a} \cdot (\vec{p_i} - \vec{p_p})$, so minimizing $J = \sum_1^N d_i$ yields $\vec{a}$ subject to $|\vec{a}| = 1$. By Lagrange multipliers, one obtains a $3 \times 3$ eigenproblem: $(M^T M)\vec{a} = \lambda \vec{a}$, where $M = [x_i^T y_i^T z_i^T]$ is the $N \times 3$ data matrix. Eventually, we get: $\sum_i (\vec{a} \cdot \vec{p_i}) = \lambda |\vec{a}|^2 = \lambda$, so minimizing $J$ is reduced to computing the minimum eigenvalue of $M^T M$. This is the square of the minimum singular value of $M$, computed by SVD, which is quite stable numerically. The corresponding singular vector is $\vec{a}$. Since the centroid of the data belongs to the plane, we can specify all parameters of the plane equation.

*Step 2*: The center and radius of rotation will be estimated by applying 2D methods. After the estimation of the best plane, the measured data are projected onto the plane. A coordinate frame is defined as follows: $\overrightarrow{a}$ is the unit vector through $p_1$, $p_n$, $\overrightarrow{n}$ is the unit normal vector of the plane, $\overrightarrow{o} = \overrightarrow{n} \times \overrightarrow{a}$. The following matrix maps the arc points from the frame of $\overrightarrow{a}, \overrightarrow{o}, \overrightarrow{n}$, to the base frame of the sensor:

$$T = \begin{bmatrix} \overrightarrow{a} & \overrightarrow{o} & \overrightarrow{n} & \overrightarrow{p_1} \\ 0 & 0 & 0 & 1 \end{bmatrix}. \tag{12}$$

Now, we have to estimate the circle in 2D. After estimation of the center and radius, the former is mapped through $T$ back to 3D space. Here we compare existing nonlinear and linear methods for 2D arc fitting. These methods are: (1) Algebraic circle fit with "hyperaccuracy", (2) Karimaki's,(3) Landau's,(4) Pratt's with SVD,(5) Riemann sphere fitting, (6) Levenberg-Marquard, (7) the Trust region,(8) Linear least squares by Kasa, and (9) Thomas' method.

The previous methods are evaluated, on a 2D arc estimation. An arc of $60^o$ is selected and normal distributed noise with standard deviation $\sigma = 0.06$ was added. As evaluation factors for the methods we selected (a) the distance between the estimated center and the actual center, (b) the difference of the estimated radius from the actual one, and (c) execution time. The Riemann sphere fitting method was more accurate and fast, because it is non-iterative and has been selected for arc fitting.

The fitting with Riemann-spheres [17], is based on the 1-to-1 mapping of a 2D circle to a Riemann sphere through stereographic projection. A circle on the Riemann sphere is its intersection with a plane in 3D, therefore the fitting of a 2D circle is reduced to fitting a plane in the Riemann sphere. The procedure is non-iterative, fast, accurate, and has 3 steps [21].

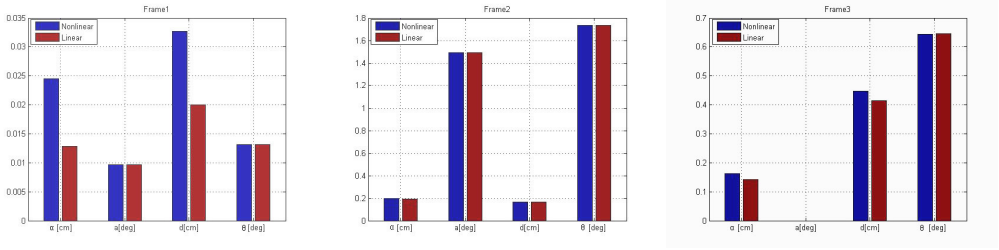


Figure 5: Simulation evaluation of the linear and nonlinear methods with noise ($\sigma = 0.04$).

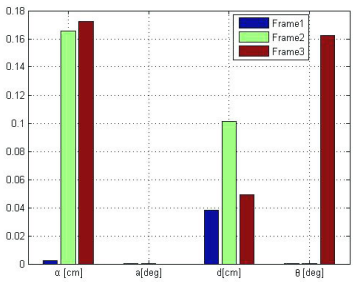


Figure 6: Experimental evaluation of the linear and nonlinear identification.

Both nonlinear and linear methods yields the equations of the 2 ankle axes. The D-H parameters can be computed geometrically based on the definition of the method [21]. **Results:** Initially the proposed method is evaluated on the model. First, the inversion-eversion motion were executed taking all the values in its range producing 41 points. Next, we fix STJ, and UAJ is rotated in its full range, producing 66 dorsiflexion/plantarflexion data of point $P_8$. Normally distributed noise with standard deviation ($\sigma = 0.04$) was added on the measured data and the simulation results are shown in fig 5. For the plane estimation of *Step 1* the observability index $O$ was evaluated on several position sets. The position set with many equally distributed points along the arc gave the maximum $O$ value. By performing SVD on the identification Jacobian we found that only the 4th singular value vanishes. Similarly, for the center estimation of *Step 2* several position sets were tested. Position set with many equally distributed points along the arc gave the maximum $O$ value. The identification Jacobian in *Step 2* has full rank and there were no non-identifiable parameters.

Our method is evaluated on an actual human foot. An adult male subject of height 1.85m and weight 80kg has been used, and the motions of the right foot were measured. For recording, we used a Microscribe 5-axes coordinate measurement device. For the dorsiflexion-plantarflexion motion, 13 positions were recorded, while for the inversion-eversion motion, we recorded 12. In comparison with the simulation results (fig. 6), the deviation between the two methods is larger which emanates from the smaller number of measurement points.

# 5 Conclusion and future work

In this thesis was studied the design and identification of kinematics parameters of robotic mechanisms for ankle physiotherapy applications. Initially, we adopted the suitable 2 axes ankle joint kinematics model from the literature and we received experimental data, in order to define a design framework for the design of a rehabilitation robot. Then, we introduced a new 2-DOF hybrid serial-parallel robot with mechanical adjustability and we performed its parametric design. This physiotherapy device outperforms to the existing physiotherapy robots on the minimum number of actuators, safety, modularity and economy. Finally, we developed a simple, robust and accurate method for identification of the ankle joint complex kinematics parameters for the appropriate tuning of a physiotherapy robot. Our method avoids the use of position tracking of multiple point-markers on the body-member and the use of expensive optical motion analysis systems. This makes it applicable in a physiotherapy clinic.

As future work, we may consider the structural study and construction of the robot. We have to investigate appropriate compliance control laws (e.g. stiffness, impedance, hybrid position/force control) [25, 26] in order to evaluate their suitability for physiotherapy operations. The development of the user software with teleoperation capabilities and operation of the platform with patients under the supervision of physiotherapist are in our interests. Also, we may revisit algebraic techniques, investigating sophisticated algorithms such as sparse interpolation, or parameter reduction so as to reduce the complexity of the resultant calculations in the kinematics parameters identification of the ankle joint complex.

# Acknowledgements

We thank Dr. C.N. Maganaris of IRM Manchester Metropolitan University for his useful advice. This work was supported by the General Secretariat of Research and Technology of Greece through a PENED 2003 program, contract nr. 70/03/8473, co-funded by the European Social Fund (75%), national resources (25%).

# References

[1] Van Den Bogert AJ, Smith GD, Nigg BM (1994). In vivo determination of the anatomical axes of the ankle joint complex: An optimization approach. J Biomech, 27:1477–1488.

[2] Craig J (1989). *Introduction to Robotics: Mechanics and Control.* Addison Wesley.

[3] Dai JS, Zhao T, Nester C (2004). *Sprained Ankle Physiotherapy Based Mechanism Synthesis and Stiffness Analysis of a Robotic Rehabilitation Device.* Autonomous Robots, (16)207-218.

[4] Daney D, Emiris IZ (2001). Robust parallel robot calibration with partial information. In Proc IEEE Intern Conf Robotics Automation, Seoul, S. Korea, pp. 3262–3267.

[5] Daney D, Emiris IZ (2004). Algebraic elimination for parallel robot calibration. In *Proc IFToMM Congress Mechanism & Mach Science*, Tianjin, China.

[6] Emiris IZ (1994). Sparse Elimination and Applications in Kinematics. PhD Thesis, Computer Science Division, Univ. of California at Berkley.

[7] Dettwyler M, Stacoff A, Kramers-de Quervaina IA, Stussi E (2004). Modelling of the ankle joint complex. Reflections with regards to ankle prostheses. Foot & Ankle Surgery., 10:109–119.

[8] Dul J, Johnson GE (1985). A kinematic model of the human ankle. J Biomedical Engineering, 7:137–143.

[9] Gamage SSHU, Lasenby J (2002). New least squares solution for estimating the average center of rotation and the axis of rotation. J Biomech 2002, 35:87–93.

[10] Girone M, Burdea G, Bouzit M, Popescu V, Deutsch JE (2001). A Stewart platform-based system for ankle telerehabilitation. Autonomous Robots, 10:203–212.

[11] Halvorsen K, Lesser M, Lundberg A (1999). A new method for estimating the axis of rotation and the center of rotation. J Biomech, 32:1221–1227.

[12] Hartenberg R, Denavit J (1955). A kinematic notation for lower-pair mechanisms based on matrices. J Appl Mech., 22:215–221.

[13] Hollerbach JM, Wampler CW (1996). The calibration index and taxonomy for robot kinematic calibration methods. Int J Robotics Research, 15:573–591.

[14] Isman RE, Inman VT (1969). Anthropometric Studies of the Human Foot and Ankle. Bulletin of Prosthetic Research, 10-11:97–129.

[15] Kim HS and Choi YJ (1999). The Kinetostatic Capability Analysis of Robotic Manipulators. in Proc. IEEE/RSJ Int. Conf. Intelligent Robots & Systems., 55-67, Korea

[16] Leitch J, Stebbins J, Zavatsky AB (2010). Subject-specific axes of the ankle joint complex. J. Biomechanics., 43:2923–2928.

[17] Lillekjendlie B (1997). Circular arcs fitted on a Riemann Sphere. Computer Vision & Image Understand., 67:311–317.

[18] Merlet J-P (2006). Parallel Robots. Springer Second Eds.

[19] Saglia J, Tsagarakis NG, Dai JS, Caldwell DG (2009). A High Performance 2-dof Over-Actuated Parallel Mechanism for Ankle Rehabilitation. Proc. IEEE Int. Conf. Robotics & Automation, Kobe, Japan, 805-809.

[20] Shakarji CM (1998). Least-squares fitting algorithms of the NIST algorithm testing system. J Res Natl Inst Stand Technol, 103:633–640.

[21] Syrseloudis CE, Daney D, Emiris IZ (2011). Identification of Kinematics Parameters of the Ankle Joint Complex. Submitted for Journal Publication

[22] Syrseloudis CE, Emiris IZ, Maganaris C, Lilas T (2008). Design framework for a simple robotic ankle evaluation and rehabilitation device. In Proc IEEE Intern Conf Engineering in Medicine & Biology, Vancouver, 4310–4313.

[23] Syrseloudis CE, Emiris IZ (2008). A Parallel Robot for Ankle Rehabilitation-Evaluation and its Design Specifications. In 8th Int. Conf. IEEE in Bioinformatics and Bioengineering, Athens, 106.

[24] Syrseloudis CE, Emiris IZ, Lilas T, Maglara A (2011). Design of a simple and modular 2-DOF ankle physiotherapy device relying on a hybrid serial-parallel robotic architecture. J Appl Bionics & Biomech, Special issue, 8:1-14.

[25] Tzafestas SG, Syrseloudis CE, Rigatos GG (2000). Hybrid Position Force Control via a Neuro-fuzzy Technique: Application to the Milling Process. *Intern. J. Mechanical Production Systems Engineering*, No 4, pp. 25-36.

[26] Tzafestas SG, Syrseloudis CE, Rigatos GG (2000). Neuro-fuzzy Hybrid Position/Force Control of Industrial Robots: A Simulation Study for the Milling Task. *3d IMACS Symp. Mathematical Modeling*, Vienna, Austria, February.

[27] Yoon J, Ryu J (2005). A Novel Reconfigurable Ankle/Foot Rehabilitation Robot. IEEE Int. Conf. Robotics & Automation. Barcelona, Spain, 2290-2295.